a NASA facsimile reproduction

OF

N70-32529

REPRODUCED FROM MICROFICHE

by the

NASA Scientific and Technical Information Facility

Technical

Technical Report
Interim Report
I-A2049-30

Report

ANALYSIS AND PERFORMANCE OF THE GAS-LUBRICATED TILTING PAD THRUST BEARING

By
W. Shapiro
R. Colsher

October 1968

Prepared Under
Contract Nonr-2342(00)
Task NR 062-316
Jointly Supported By
Department of Defense
Atomic Energy Commission
National Aeronautics and Space Administration

Administered by
Office of Naval Research
Department of the Navy

THE FRANKLIN INSTITUTE RESEARCH LABORATORIES
BENJAMIN FRANKLIN PARKWAY • PHILADELPHIA, PENNA. 19103

ABSTRACT

The inherent self aligning capability and superior resistance to thermal distortion, of the gas-lubricated tilting-pad thrust bearing,could often offset load capacity limitations and make it an attractive compromise for many applications. A numerical treatment for analyzing the tilting-pad thrust bearing is presented along with extensive performance information for a particular pad geometry. An optimum hydrodynamic crown profile and related dimensions are determined. The range of validity of incompressible theory and the rectangular approximation are also developed.

TABLE OF CONTENTS

LIST OF FIGURES

NOMENCLATURE

c = clearance of aligned pad above high point of crown, in.

C_L = dimensionless load coefficient = $\frac{w}{p_a r_o^2}$

F = viscous friction moment factor = $\frac{m_f}{p_a r_o^{2} o}$

H = dimensionless film thickness, h/c

H_{min} = dimensionless minimum film thickness = h_{min}/c

H_p = dimensionless pivot film thickness = h_p/c

h = local film thickness, in.

h_{min} = minimum film thickness, in.

h_p = pivot film thickness, in.

HP = viscous friction horsepower loss

M_x = dimensionless moment about radial axis = $\frac{m_x}{p_a r_o^3}$

M_y = dimensionless moment about axis normal to radius through point of tilt = $\frac{m_y}{p_a r_o^3}$

m_f = viscous friction moment, in-lbs

m_x = moment about radial axis, in-lbs

m_y = moment about axis normal to radius through point of tilt, in-lbs

P = dimensionless pressure = p/p_a

p = local pressure, psia

p_a = ambient pressure, psia

Q = independent variable = P^2

R = dimensionless radius = r/r_o

R_m = dimensionless mean radius = r_m/r_o

R_{pv} = dimensionless radius to pivot (center of pressure) = $\frac{r_{pv}}{r_o}$

r = radius, in.

r_i = pad inside radius, in.

r_m = mean radius, in.

r_o = pad outside radius, in.

r_{pv} = radius to pivot (center of pressure), in.

r' = radius to point where pad is tilted, in.

T = dimensionless time = $\frac{\omega_1 t}{2}$

t = time, seconds

W = pad load, lbs.

W_t = total bearing load, lbs.

α = tilt about radial line, rad

α_θ = tilt about axis normal to radius through point of tilt. rad.

α_r = tilt about radial line, = α, rad

γ = angle between leading edge and pivot (center of pressure), rad.

δ = crown height, in.

ζ = radius of curvature of pad, in.

θ = angular coordinate, rad

θ_p = angular extent of pad, rad.

θ' = angle to point where pad is tilted, rad

θ_o = angle to leading edge of pad, rad

Λ = compressibility parameter = $\frac{6\mu\omega r_o^2}{p_a c^2}$

μ = absolute viscosity, lb-sec/in^2

ω = shaft speed, rad/sec

ω_1 = reference speed = $\frac{2T}{t}$, rad/sec

1. INTRODUCTION

Dishing or crowning of bearing surfaces due to viscous heat generation can seriously degrade load capacity of single surface thrust bearings.(1)* In addition, complex alignment schemes (gimbals, etc.) are often necessary to compensate for the distortion of the housing to which the thrust bearing is attached. The self-equalized tilting pad thrust bearing with inherent self-alignment and reduced tendency to thermally distort, then becomes an attractive compromise. Use of this bearing with compressible fluids has been retarded, ostensibly because of poor load capacity, but when comparisons are made with imperfect geometries resulting from thermal or structural deformations, the tilting pad bearing could be a better choice. Also, comparisons are generally made on the basis of equal minimum film thickness, an unfair criterion to the tilting pad bearing, since automatic adjustment of the tilt is an added safety factor; i.e., safe operation can be achieved at lower minimum film thickness than with the single surface variety.

This paper presents the pertinent results of investigations of the sectored crowned profile pad. Included are optimization criteria, design information and procedures and limitations of some of the common approximations.

*Superscripted numerals identify references.

2. THEORETICAL FOUNDATIONS

Governing Equations

For isothermal films the compressible Reynolds' equation in polar coordinates is

$$\frac{\partial}{\partial r}\left(\frac{rph^3}{\mu}\frac{\partial p}{\partial r}\right) + \frac{1}{r}\frac{\partial}{\partial \theta}\left(\frac{ph^3}{\mu}\frac{\partial p}{\partial \theta}\right) = 6r\omega\frac{\partial(ph)}{\partial \theta} + 12r\frac{\partial(ph)}{\partial t} \tag{1}$$

By a change of independent variable and non dimensionalization the following equation results:

$$\frac{\partial}{\partial R}\left(\frac{RH^3}{2}\frac{\partial Q}{\partial R}\right) + \frac{1}{R}\frac{\partial}{\partial \theta}\left(\frac{H^3}{2}\frac{\partial Q}{\partial \theta}\right) = \Lambda R\left[\frac{\omega}{\omega_1}\left(\sqrt{Q}\frac{\partial H}{\partial \theta} + \frac{H}{2Q}\frac{\partial Q}{\partial \theta}\right) + \sqrt{Q}\frac{\partial H}{\partial T} + \frac{H}{2\sqrt{Q}}\frac{\partial Q}{\partial T}\right] \tag{2}$$

$Q = P^2$ has been selected as the independent variable because for configurations such as a Rayleigh Step, that contains discontinuities in the film thickness distribution, it is a more convenient independent variable than the usual P^2H^2. Although Rayleigh Steps are not considered here the desire for generality of the final computer program dictated the use of P^2 as the independent variable.

Paradoxically, the time dependent terms are maintained in equation (2), though the immediate interest is for steady-state information. The reasoning is that regardless of whether the time dependent terms are maintained, the resulting equation is non-linear and some sort of iterative scheme is required to obtain a solution. Steady-state data is derived by diffusing the pressure field as a function of time until variations in pressures between successive time intervals do not differ by more than a specified truncation error. The advantage of preserving the transient terms in the governing equations is that steady-state information is generated at no loss in efficiency and the option of conducting future dynamic studies is available.

Another significant item concerning equation (2) is the use of the variable ω/ω_1. The compressibility parameter Λ and time T are non-dimensionalized with the reference speed ω_1, rather than the slider velocity ω. If ω was used for non-dimensionalizing, then all terms of the right hand side of equation (2) would be obliterated at zero slider velocity, and it would not be possible to obtain pure squeeze film effects. Thus, with slider velocity, ω/ω_1 equals unity, otherwise the parameter equals zero.

Equation (2) is expanded by finite difference and combined into a general matrix equation of the form(2)

$$[C_j]\{Q_j\} + [D_j]\{Q_{j-1}\} + [E_j]\{Q_{j+1}\} = \{F_j\}$$

$$j = 1, N \tag{3}$$

For interior points the $[C_j]$ matrix is tri-diagonal and $[D_j]$ and $[E_j]$ are diagonal. The non-linearities occur because the coefficient matrices and the right hand side vector are functions of the $\sqrt{Q}$.

The boundary conditions are satisfied by manipulation of the coefficients and the right hand side of equation (3). Thus, for ambient pressures on the boundary

$$[D] = [E] = 0$$

$$\{F\} = \{1\}$$

$$\text{and} \quad C_{ik} = \delta_{ik} \quad \text{(kronocher delta)} \tag{4}$$

The coefficient matrices of equation (3) are also functions of the clearance distributions which depends upon the type of convex profile. Section 5 describes the three hydrodynamic crown profiles examined. With regard to film thickness distribution, the following expressions apply (See Figure 1).

GENERAL

$$H_{ij} = 1 + Z_s + H' + \frac{r_o\alpha_\theta}{c}\left[R_i\cos\left(\theta' - \theta_j\right) - R'\right] - \frac{r_o\alpha_R}{c}R_i\sin\left(\theta' - \theta_j\right) \tag{5}$$

PARABOLIC

$$H' = 4\,\delta/c\left[\frac{\theta_j - \left(\theta_o + \theta_{p/2}\right)}{\theta_p}\right]^2 \tag{5-a}$$

CYLINDRICAL

$$\zeta/c = \left(\frac{r_o}{c}\right)^2\frac{R_m^2\sin^2\left(\theta_{p/2}\right)}{2\delta/c} + \frac{1}{2}\delta/c \tag{5-b}$$

$$H' = \zeta/c - \left\{(\zeta/c)^2 - \left[\frac{r_o}{c}R_i\sin\left(\theta_j - \theta_{p/2} - \theta_o\right)\right]^2\right\}^{1/2} \tag{5-c}$$

R_m = mean radius

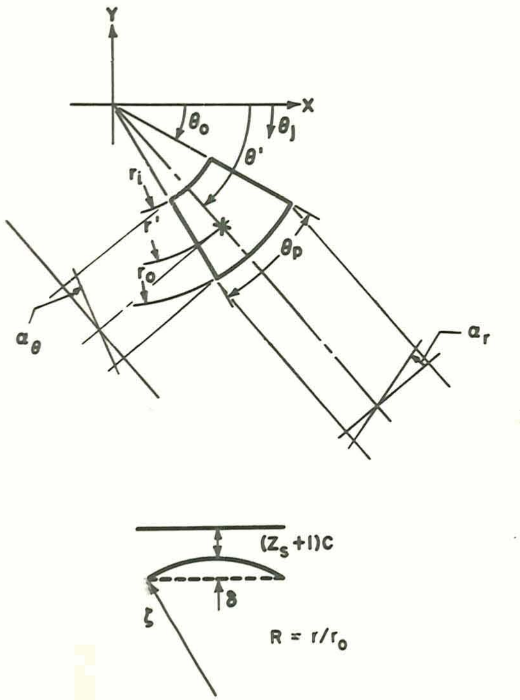

Fig. 1 Geometric Variables for Generation of Film Thickness Distribution

SPHERICAL

$$\zeta/c = \frac{\left[R_m^2 + R_m'^2 - 2R_m R_m' \cos\left(\theta_{p/2}\right)\right]\left(\frac{r_o}{c}\right)^2 + \left(\zeta/c\right)^2}{2\delta/c}$$

where

$$R_m = R_m/(\cos\theta_{p/2}) \tag{5-d}$$

$$H' = \zeta/c - \left\{(\zeta/c)^2 - \left[R_i^2 - R_m'^2 + 2R_i R_m' \cos(\theta_j - \theta_{p/2} - \theta_o)\right]\left(\frac{r_o}{c}\right)^2\right\}^{1/2} \tag{5-e}$$

For the cylindrical and spherical profiles the radius of curvature enters into the film thickness expression, while for the parabolic it does not appear. This is manifest in the final expression for film thickness by the variable r_o/c. Fortunately, as demonstrated later, the results are extremely insensitive to the effects of this variable so that it does not complicate parametric studies.

c is defined as the original clearance above the highest point or line of the crown, with the pad in the uninclined position. It is used as a non-dimensionalization parameter. For any particular set of operating conditions it is convenient to maintain c a constant so that non-dimensionalization parameters are unaffected by variations in operating film thickness. The parameter Z_s is used to vary the uninclined film thickness without changing c.

The column-matrix method of solution of equation (3) has been treated in reference 2. It basically consists of letting

$$\{Q_{j-1}\} = [A_j]\{Q_j\} + \{B_j\}$$

$$j = N \to 2 \tag{6}$$

Substituting (6) into (3) and solving for $\{Q_j\}$ produces

$$\{Q_j\} = -\left[[C_j] + [D_j][A_j]\right]^{-1}[E_j]\{Q_{j+1}\}$$

$$= -[T]^{-1}\left[[D_j]\{B_j\} - \{F_j\}\right] \tag{7}$$

where

$$[T] = [C_j] + [D_j][A_j]$$

Comparing (6) and (7)

$$[A_{j+1}] = -[T]^{-1}[E_j]$$

$$[B_{j+1}] = -[T]^{-1}\left[[D_j]\{B_j\} - \{F_j\}\right] \tag{8}$$

Note from boundary conditions $\{Q_1\} = \{1\}$ which implies that

$$[A_2] = 0, \ \{B_2\} = \{1\} \tag{9}$$

Equation (9) is the starting point for the recursion relations of equation (8), and subsequent formation of the matrices [A] and [B].

For each time step the non-linearity introduced by the parameter $\sqrt{Q}$ in the coefficient matrices and right side is removed by computing its value from the previous iteration, and then solving the resultant linear equation. A simplified flow chart for the solution process is shown on Figure 2. Equations (10) through (13) are for thrust load capacity, righting moments, and viscous friction drag respectively.

$$C_L = \int_{r_i/r_o}^{1} \int_{o}^{\gamma} (P-1) \ R d\theta dR \tag{10}$$

$$M_x = \int_{r_o/r_o}^{1} \int_{o}^{\gamma} (P-1) \ R^2 \sin \theta d\theta dR \tag{11}$$

$$M_y = \int_{r/r_o}^{1} \int_{o}^{\gamma} (P-1) \ R^2 \cos \theta d\theta dR \tag{12}$$

The effect of the viscous drag on the shaft is evaluated from

$$F = \int_{r_i/r_o}^{1} \int_{o}^{\gamma} \frac{H}{2} \frac{\partial P}{\partial \theta} R d\theta dR + \frac{\Lambda\omega}{6\omega_1} \int_{r_i/r_o}^{1} \int_{o}^{\gamma} \frac{R^3}{H} d\theta dR \tag{13}$$

The above equations are for one pad. When multiple pads are considered each pad is handled separately and the results consecutively added.

SIMPLIFIED FLOW CHART

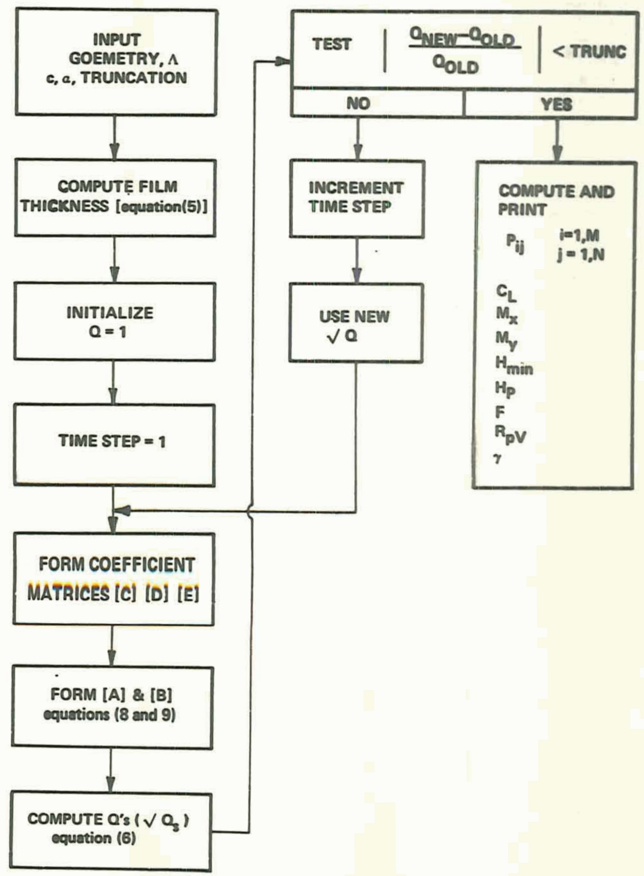

Fig. 2 Simplified Flow-Chart Computer Program

3. GEOMETRIC VARIABLES

Figure 3 shows the pertinent geometric variables concerned with the subsequent information to be presented. The parameters r_{pv} and γ locate the position of the pad pivot point. For any particular operating condition this point corresponds to the center of pressure. Note that this point is different from the origin of tilt (r', θ') which is prespecified and required to generate the inclined film thickness distribution. The center of pressure is necessarily obtained after determination of the pressure field and is thus program output. For all future studies the pad was inclined about a radial line through the center of the pad by an amount $\alpha = \alpha_r$. (tilts in α_θ direction were not studied. See Figure 1). Also, the reference clearance c is redefined as the film thickness along the mid radius at the specified r′ prior to inclining the pad. (The variable Z_s (Figure 1) is now absorbed in c.)

Some dimensionless parameters are defined in two ways. When investigating optimum crown height then it is convenient to maintain c a constant and vary δ. Then c is used as a reference length. When investigating performance of a specific pad geometry over a range of film thicknesses, then the crown height δ is used as a reference length and replaces c in such parameters as Λ, $\frac{\alpha r_o}{c}$ and $\frac{h}{c}$ etc.

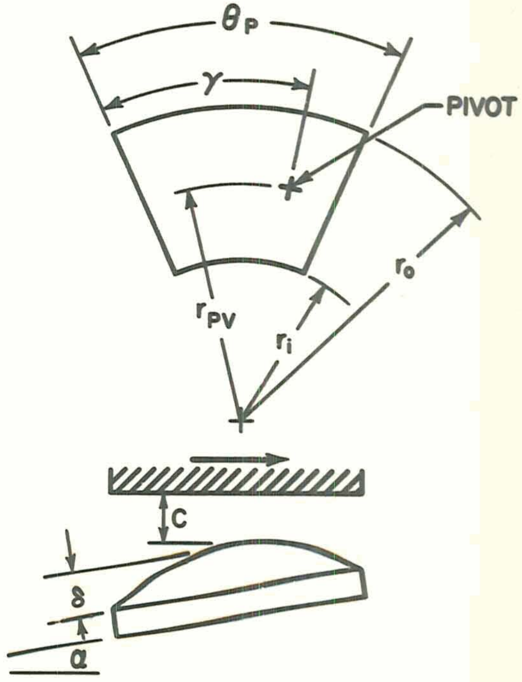

Fig. 3 Definition of Geometry for Performance Plots

4. ANALYTICAL VALIDATION

The analysis was checked against published information, and against results of an independent analysis using different techniques. Gross[3] produced results for a rectangular slider with a convex profile. To approximate this situation with the present analysis, that considers a pie shaped sector, it was necessary to use large inside and outside radii and maintain the difference between them at the correct slider width. The tabulation shown on Figure 4 shows the comparative results of the pressure in the x direction at y = 0. Also shown is the comparative results of total load. The comparisons are excellent. As a sector pad approaches a rectangle the film thickness distributions for the parabolic and cylindrical profile should approach each other. Indeed, computer runs were made for both these profiles with identical results.

The second check was made against another numerical analysis that computes performance of rectangular sliders. Identical grid sizes were used for both cases. The numerical approach is different however, in that the rectangular pad method iterates on an explicit equation for the pressure distribution. The dashed lines on Figure 5 are pressure variations for the explicit solution, while the solid lines are results from the matrix column (implicit) method. Again for the present analysis that treats a sector, the rectangular shape was obtained by using large radii. Along the row I = 8, the pressure for both analyses follow identical distributions except at the peak pressure points. Along the column J = 8, which is the mid column, the pressures are identical. At the column J = 14, the explicit analysis gives slightly lower pressures. The explicit solution converges asymptotically, while the matrix column approach straddles the solution and converges much more rapidly to the correct solution. Irrespective, the comparisons are good and the correctness of the program substantiated.

TILTING PAD THRUST BEARING

CHECK CASE (CROWNED SLIDER)

Y = 0

X	P GROSS	P PROGRAM (PARABOLIC; CYLINDRICAL)
0	1.0	1.0
2	1.13	1.12
4	1.26	1.26
6	1.40	1.41
8	1.58	1.58
10	1.69	1.68
12	1.0	1.0

W' Gross = $\frac{W}{BLPa}$ = 0.2722

W' Computer = 0.2719

h_2 Gross = 0.0005 in

h_2 Computer = 0.0005 in

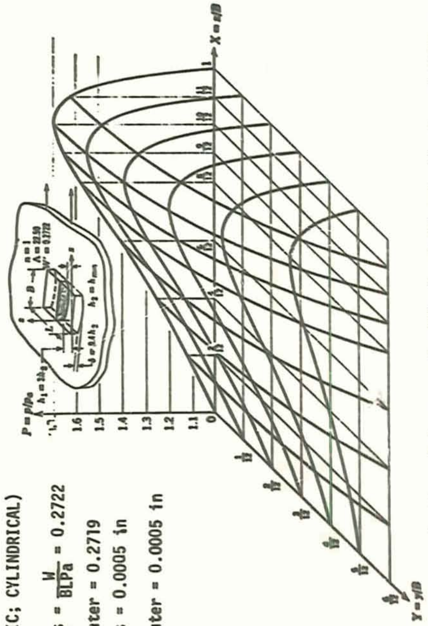

Isothermal Pressure Profile for Cylindrically Curved Slider, Λ = 22.50, W' = 0.2722, L' = 1, H_1 = 3, δ/h_2 = 0.4, h_2/h_m = 1.

(From Reference 3)

Fig. 4 Comparative Results between Gross[3] and Computer Program

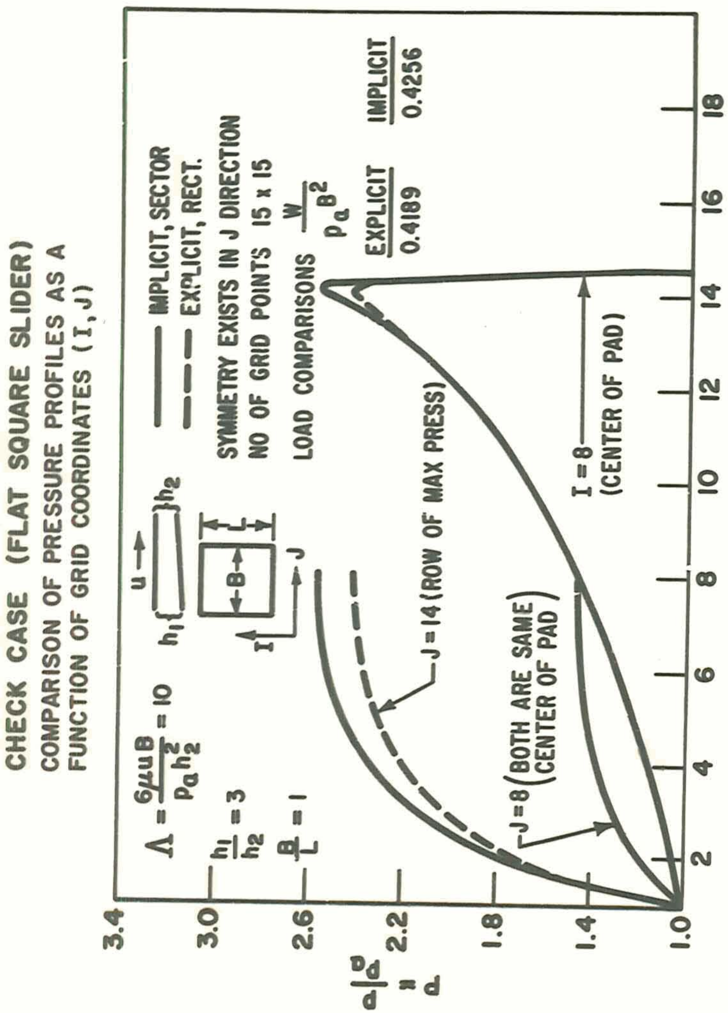

Fig. 5 Comparative Results, Explicit Solution of a Flat Slider Versus Implicit (Matrix Column) Method

5. HYDRODYNAMIC PROFILES

To provide a converging wedge at startup, and to improve load capacity it is advantageous to shape the sector with a convex crown.

Three crown profiles were examined:

(a) Parabolic – The crown follows a parabolic curve along a circumferential line. The maximum crown height occurs along a radial line through the center of the pad and is the reference crown height for this configuration. When the pad is at zero inclination angle the crown height along any radial line does not vary. (Figure 6a)

(b) Cylindrical – The cylindrical crown is formed by removing a pie shaped sector from a cylinder. The crown height increases along a radial line from inside to outside radius. The height at the geometric center of the pad is taken as the reference crown height. (Figure 6b).

(c) Spherical – The spherical profile is formed such that the four pad corners lie on the same latitude circle. The pole position is taken as the location for the reference crown height. (Figure 6c).

Film thickness expressions for these crown profiles were described in equation 5.

Studies of the profiles were made for the two conditions of primary interest.

(1) Performance variations for constant crown height, δ and varying film thickness, c.

(2) Performance variations for constant film thickness, c and varying crown height, δ

Figure 7 shows load, friction, and minimum film thickness as a function of the pivot position, for condition (1). Note that Λ is defined with the constant parameter δ which replaces c for non-dimensionalization. Three sets of curves are shown for varying values of δ/c, which indicates varying film thickness c. As δ/c is reduced or as c increases the load capacity decreases, the minimum film increases, and the viscous friction decreases. These results are as expected. The cylindrical profile has superior load capacity and film thickness. Figure 8 shows results of condition (2). Since c is a constant, Λ as defined with δ varies as δ/c varies. Again, the cylindrical profile shows superior load capacity and film thickness. Figure 9 is an expanded plot of a set of curves on Figure 8. It is typical for both conditions (Figures 7 & 8) and it demonstrates conclusively the advantage of the cylindrical profile. For equal load coefficients the cylindrical profile provides a thicker film than either the parabolic or spherical crowns. The spherical crown exhibits slightly less viscous friction but this is insufficient to challenge the advantages of the cylindrical profile.

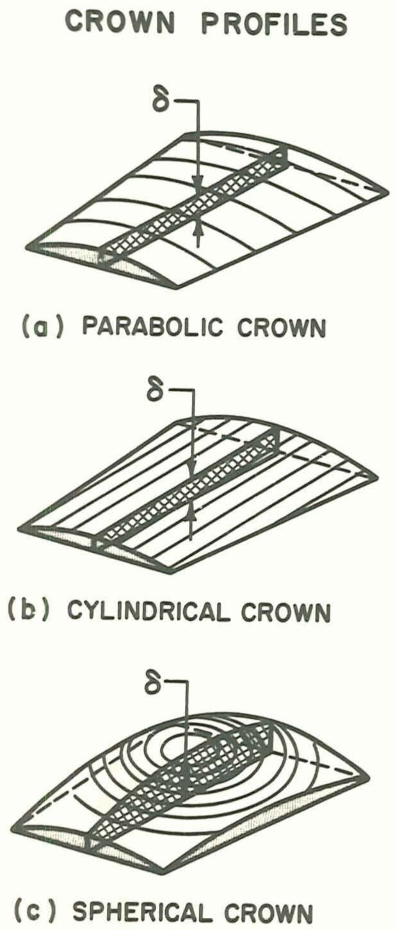

Fig. 6 Crown Profiles

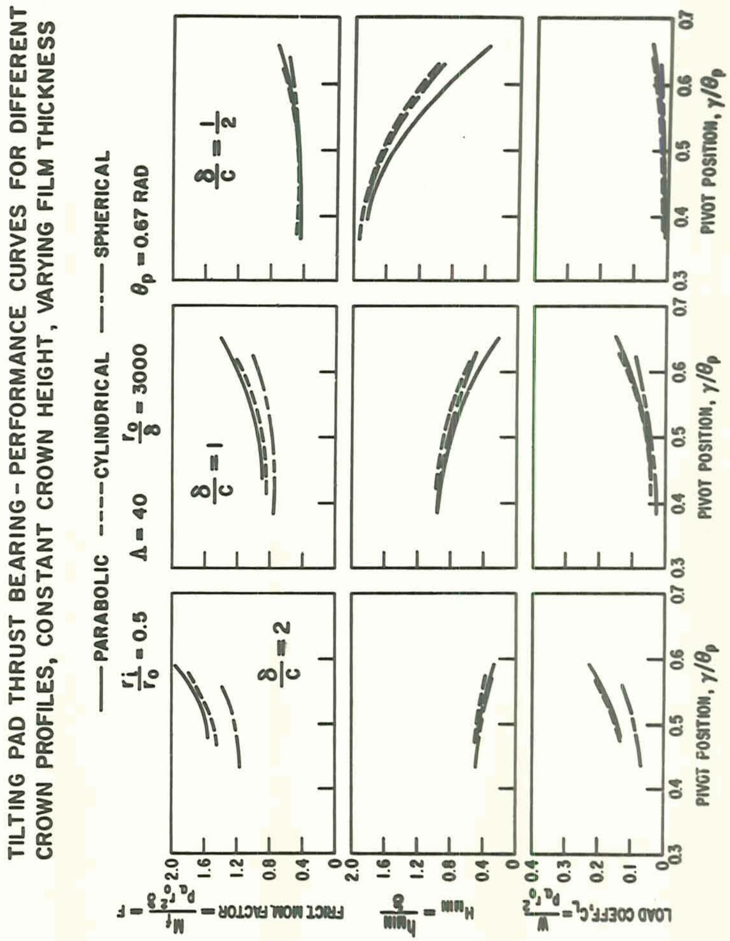

Fig. 7 Crown Profile Performance, Constant Crown Height, δ Varying Film Thickness, c

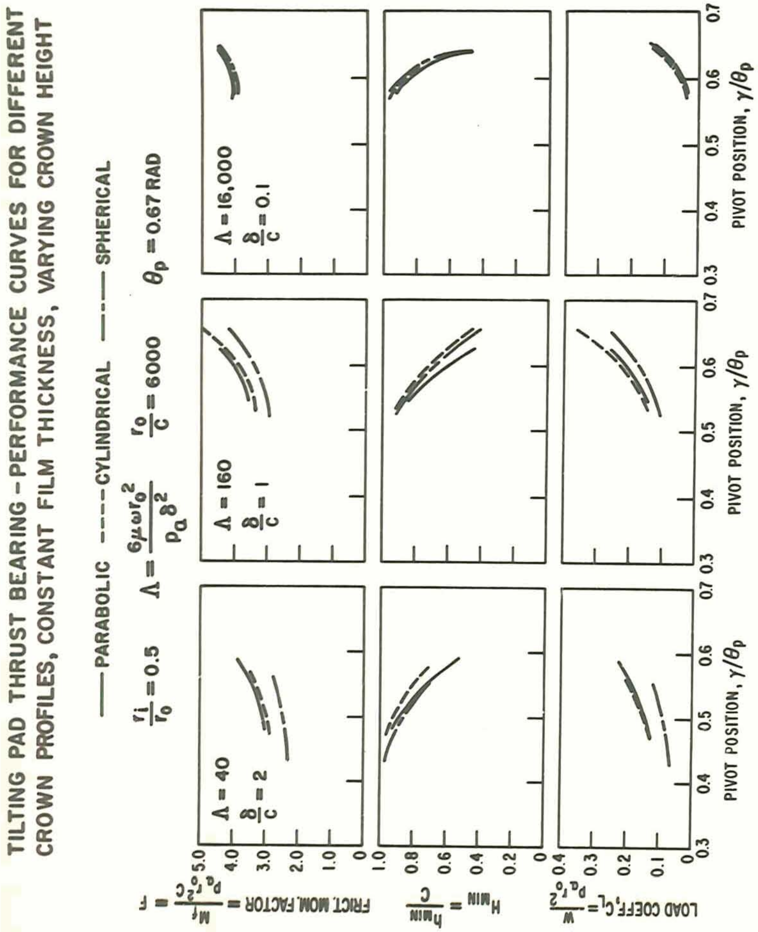

Fig. 8 Crown Profile Performance, Constant Reference Clearance c, Varying Crown Height, δ

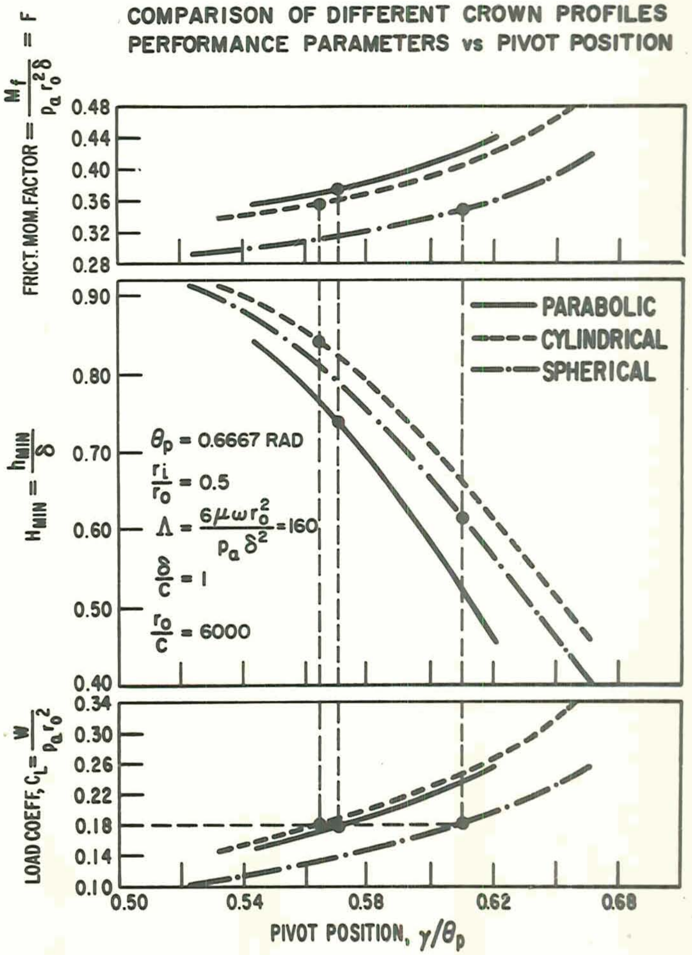

Fig. 9 Comparison of Different Crown Profiles, Performance Parameters vs. Pivot Position

Figure 10 are isobar plots of the three crowns at a particular value of Λ and inclination. The parabolic crown has the smallest film thickness, while the cylindrical has the largest. The ratio of load to minimum film however, is much larger for the parabolic than for the cylindrical profile. Because of the demonstrated advantages of the cylindrical profile, further studies were restricted to the cylindrical crown profile, except for comparisons between compressible and incompressible theory, where it was more convenient to use the parabolic profile.

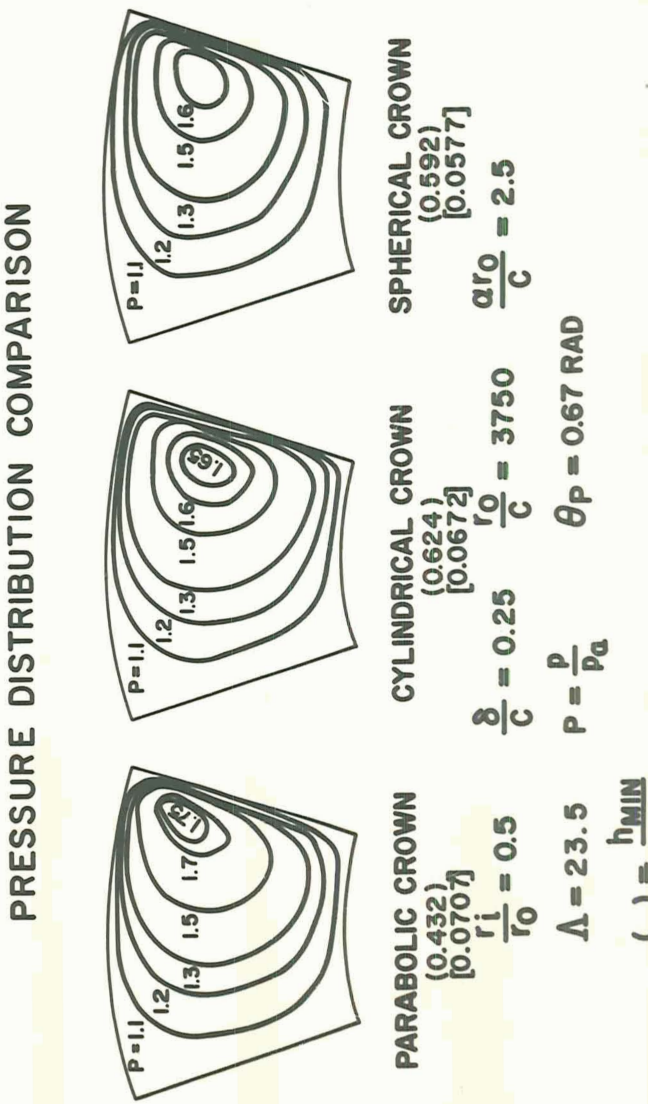

Fig. 10 Isobar Plots of Crown Profiles at Equal Inclinations

6. VARIATION OF PERFORMANCE WITH PARAMETER r_o/c

The film thickness expression for the cylindrical and spherical crown profiles contain the parameter r_o/c or r_o/δ if the crown height is selected as the reference clearance. The parabolic profile does not contain this parameter. Examination of the comparative results of the three profiles however, do not reveal a marked difference among them. The significance of r_o/c then becomes suspect, and if it can be removed as a variable, parametric studies become less complicated.

Studies to determine the effect of r_o/δ were conducted for various values of Λ crown height and pad tilt, and Table 1 is a sampling of results. It is evident that performance is very insensitive to the variable r_o/δ, and it need not be considered significant for parametric studies.

TABLE 1

TILTING PAD THRUST BEARING - VARIATION OF PERFORMANCE WITH PARAMETER r_o/δ

$\Lambda = 250$, $\delta/c = .25$, $\frac{\alpha\, r_o}{\delta} = 6.0$

r_o/δ	$\gamma/\theta p$	r_{pv}/r_p	Hp	H_{MIN}	Frict. Coeff.	C_L
2500	0.53611	0.76173	3.8761	3.2586	1.9088	0.037058
5000	0.53565	0.76175	3.8776	3.2586	1.9088	0.036908
7500	0.53611	0.76173	3.8761	3.2586	1.9088	0.037058
10000	0.53611	0.76173	3.8761	3.2586	1.9088	0.037058

$\Lambda = 250$, $\delta/c = 1$, $\frac{\alpha\, r_o}{\delta} = 3$

r_o/δ	$\gamma/\theta p$	r_{pv}/r_p	Hp	H_{MIN}	Frict. Coeff.	C_L
2500	0.56832	0.76676	0.89716	0.81468	6.5514	0.26515
5000	0.56832	0.76676	0.89716	0.81468	6.5514	0.26515
7500	0.56828	0.76674	0.89720	0.81468	6.5515	0.26514
10000	0.56828	0.76674	0.89720	0.81468	6.5515	0.26514

$\Lambda = 25$, $\delta/c = 1$, $\frac{\alpha\, r_o}{\delta} = 3$

r_o/δ	$\gamma/\theta p$	r_{pv}/r_p	Hp	H_{MIN}	Frict. Coeff.	C_L
2500	0.50407	0.75665	0.99281	0.81468	0.70054	0.05722
5000	0.50407	0.75665	0.99281	0.81468	0.70054	0.05722
7500	0.50407	0.75665	0.99281	0.81468	0.70054	0.05722
10000	0.50407	0.75665	0.99281	0.81468	0.70054	0.05722

$$\Lambda = \frac{6\mu\omega r_o^2}{P_a\,\delta^2}$$

$\theta_p = 0.7854$

$r_i/r_o = 0.5$

7. POSITION OF PIVOT

A by product of the pie sector pad analysis is determination of the radial position of the pivot. The rectangular approximation eliminates this parameter and the location is usually taken at the mean radius. The results of the analysis prove that the radial position is very insensitive to film thickness, crown height, inclination and compressibility parameter Λ. Table 2 shows some tabulated results. The largest variation is 5%, and the mean radial position (R_m = 0.75) is not very far from the correct value. The actual position is slightly outboard of the mean radius. Although the hydrodynamic velocities are greater toward the outer radius, the restriction to flow is less because of the greater escape area. The counter-balancing effects maintains the radial position of the pivot near the mean radius and limits the variation to a narrow range. The radial pivot location should be satisfied for normal operating conditions so that a pure pitching of the pad is effected. Because of the insensitivity of the radial pivot position, rolling of the pad at off design conditions should not be significant.

TABLE 2

TILTING PAD THRUST BEARING - VARIATION OF RADIAL PIVOT LOCATION

Λ = 25

δ/c	$\alpha\, r_o/\delta$	r_{pv}/r_o
0.25	1.0	0.80926
	2.0	0.77013
	3.0	0.76211
	4.0	0.75997
	6.0	0.76027
	8.0	0.76356
	12.0	0.78112
	14.0	0.80451
0.50	1.0	0.78786
	2.0	0.76398
	3.0	0.75826
	4.0	0.75735
	6.0	0.76271
	8.0	0.77814
	9.0	0.79453
	9.75	0.80979
1.0	1.0	0.76742
	2.0	0.75879
	3.0	0.75665
	4.0	0.75829
	6.0	0.77420

Λ = 250

δ/c	$\alpha\, r_o/\delta$	r_{pv}/r_o
0.25	0.5	0.78677
	1.0	0.77348
	2.0	0.76407
	4.0	0.76051
	6.0	0.76175
	8.0	0.76525
	10.0	0.77095
	12.0	0.77962
	14.0	0.78908
0.50	0.5	0.77200
	1.0	0.76776
	3.0	0.76231
	6.0	0.76656
	8.0	0.77544
1.0	0.5	0.77654
	1.0	0.77269
	2.0	0.76840
	3.0	0.76676
	4.0	0.76721
	5.0	0.76984
	6.0	0.77693

Λ = 2500

δ/c	$\alpha\, r_o/\delta$	r_{pv}/r_o
0.25	0.5	0.78204
	1.0	0.77812
	2.0	0.77481
	3.0	0.77329
	4.0	0.77270
	6.0	0.77298
	8.0	0.77361
	12.0	0.77974
0.50	0.5	0.78807
	1.0	0.78455
	2.0	0.78178
	3.0	0.77986
	4.0	0.77915
	6.0	0.78063
1.0	0.5	0.78660
	1.0	0.78869
	2.0	0.78459
	3.0	0.78257
	4.0	0.78212

$\Lambda = \frac{6\mu\omega r_o^2}{p_a \delta^2}$, $\frac{r_i}{r_o} = 0.5$, $\theta_p = 0.7854$

8. OPTIMUM CROWN HEIGHT

A primary geometric parameter needed to select a pad configuration is the value of the crown height. A series of runs were made at different values of the compressibility parameter Λ maintaining the reference clearance c a constant and varying the crown height δ. Since c is the constant parameter it is used in the definition of Λ, rather than δ. The values of Λ investigated were 25,100 and 250, and δ/c was varied between 0 and 2. This represents a broad range of parameters and sufficient information is obtained to make decisions regarding optimization of the crown height. Figures 11, 12, and 13 show the variation of Load Coefficient, Friction Moment Factor and Circumferential Pivot Position as a function of δ/c. The Minimum Film Thickness is used as a family parameter. Since the Minimum Film Thickness is program output, the information in Figures 11, 12, and 13 could not be obtained directly but required a considerable amount of cross plotting. The significant conclusions of these results are as follows:

(1) Except at very small minimum films, performance is rather insensitive to crown height for values of δ/c between 0.8 and 1.5.

(2) The circumferential pivot position is almost invariant with the value of the crown height.

(3) A good selection for the value of δ/c would be unity, since it provides near optimum load capacity over a broad range of film thicknesses and values of the compressibility parameter Λ.

(4) As Λ increases the pivot position has a tendency to move closer to the trailing edge and the range of values of the pivot position is reduced. Pivot positions between 0.5 and 0.6 give reasonable values of minimum film thickness.

(5) A crown considerably improves performance over a flat slider as can be seen by noticing the difference in performance between $\delta/c = 0$ and $\delta/c = 1$. For example, for $H_{min} = .6$, the load capacities are at least doubled, and a more noticeable improvement is noted at the higher Λ values. Also, except for very low values of film thickness, the viscous friction is slightly less for the crowned profile than for the flat slider.

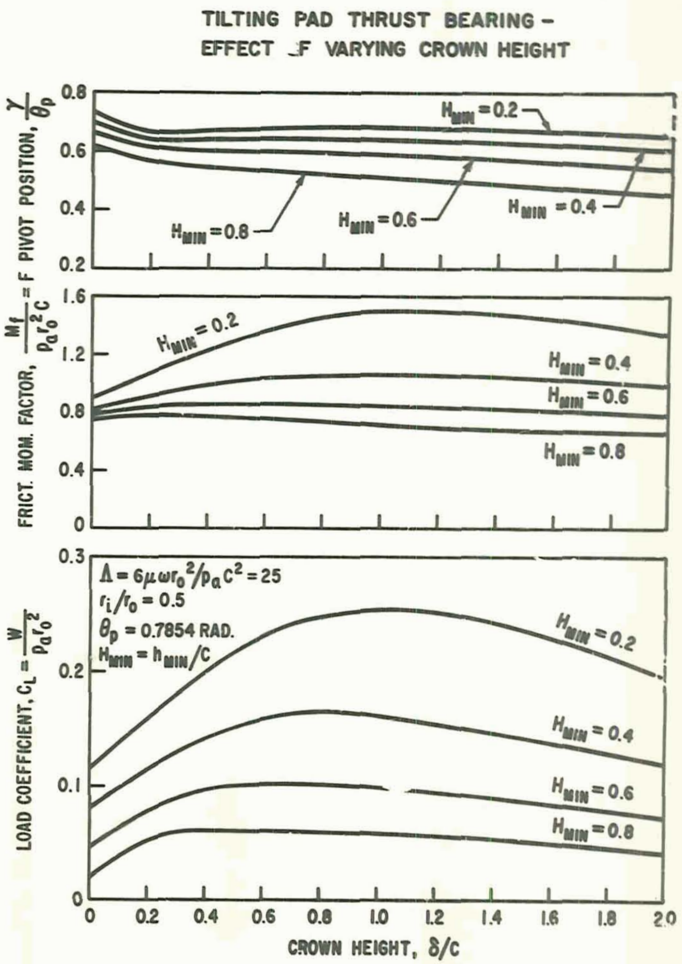

Fig. 11 Variation of Performance with Crown Height, $\Lambda = 25$

TILTING PAD THRUST BEARING –
EFFECT OF VARYING CROWN HEIGHT

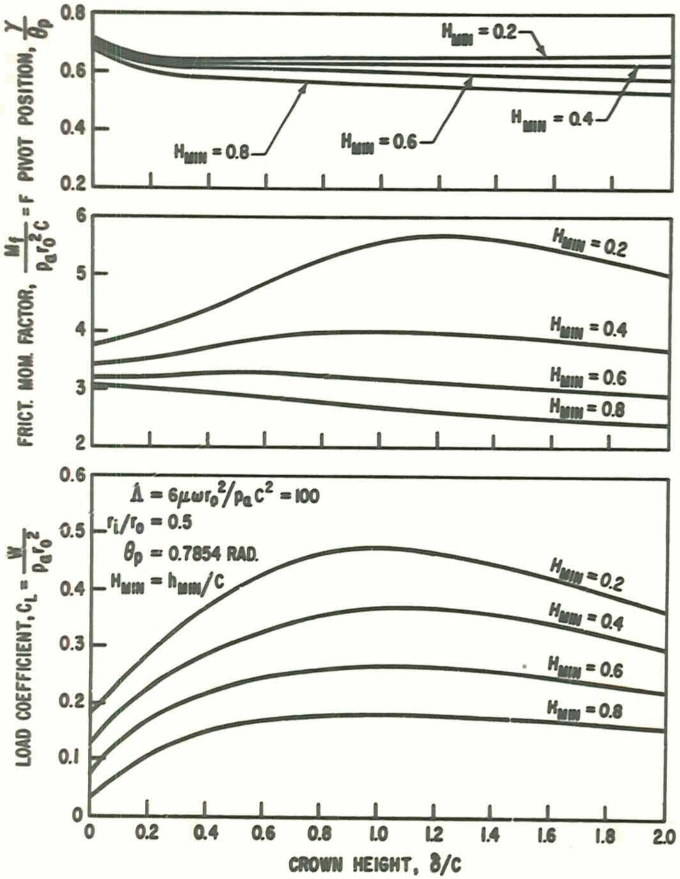

Fig. 12 Variation of Performance with Crown Height, Λ = 100

TILTING PAD THRUST BEARING –
EFFECT OF VARYING CROWN HEIGHT

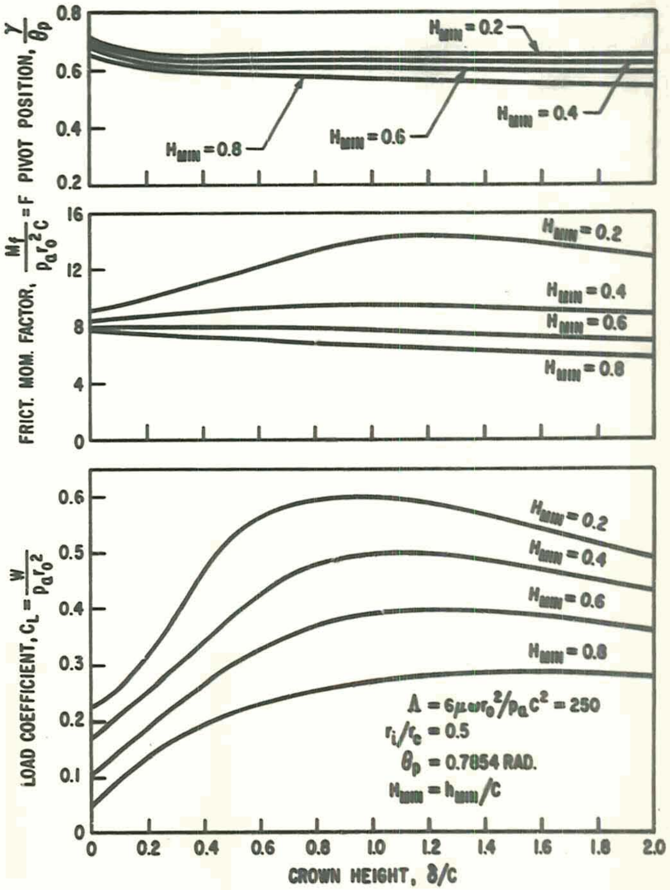

Fig. 13 Variation of Performance with Crown Height, Λ = 250

9. PERFORMANCE FIELD PLOTS

Field plots were developed for the purpose of determining performance of a sectored pad with a specific crown height and varying film thickness. The pivot position can be pre-specified, or alternatively can be optimized for specific operating conditions. Since for these plots the crown height is constant it is taken as the reference length in the definitions of Λ and other dimensionless parameters. The plots consist of Load Coefficient C_L, Minimum Film Thickness H_{min} Friction Moment Factor, F, and Pivot Film Thickness H_p, as a function of pivot position γ/θ_p. The crown height to clearance ration, δ/c and pad tilt, $\alpha r_o/\delta$, are family parameters. Three values of Λ were considered 25, 250, and 2500, respectively. The field plots provide extensive information for the particular pad geometry considered.

The curves for $\Lambda = 25$ (Figures 14 and 15) are representative of small Λ or nearly incompressible operation. The operating pivot position is spread over a fairly wide range. As the film thickness decreases or δ/c increases, variations of load coefficient are quite sensitive to pivot position.

In order for film thicknesses to be maintained at reasonable levels, and insure adequate load capacity it would appear that the pivot position should be maintained between 0.5 and 0.6. Then, for an operating $\delta/c = 1$ the minimum film would not be less than ½ of the crown height. Also, the value of $\delta/c = 1$ should be selected for maximum load conditions if variable loads will be encountered. Figure 15 shows Friction Moment Factor and the Pivot Film Thickness as a function of pivot position. The viscous friction also shows a sharp increase at higher values of pivot position, due to the reduction in film thickness. Pivot film thicknesses are not as sensitive as minimum films for any constant value of δ/c, and varying pivot position. Again, the more acute variations occur at the higher pivot positions.

Figures 16 and 17 are the field plots at $\Lambda = 250$. For most applications, this value of Λ is well into the compressible region. The overall field plot is much more compressed (narrower range of pivot positions) than for the low Λ case. This was also evident in the varying crown height curves, Figures 11, 12 and 13.

The values of load coefficient are almost an order of magnitude higher than for the low Λ situation reflecting the higher hydrodynamic pressures generated by increased velocities. Pivot positions in the range between 0.5 and 0.65 would appear to provide reasonable load capacities and minimum films. The Friction Moment Factor is much higher for the higher Λ case differing by an order of magnitude.

The field plots for $\Lambda = 2500$ are shown on Figures 18 and 19. These curves represent operation considerably into the compressible range to the extent that load capacity should not be very much improved over operation at much lower Λ's.

There is slight improvement in load capacity and minimum film as compared to the $\Lambda = 250$ case, but the difference is not nearly as much as that between $\Lambda = 250$ and $\Lambda = 25$. The improvement is obtained by paying an incommensurate price in viscous friction losses which are an order of magnitude higher than for $\Lambda = 250$.

TILTING PAD THRUST BEARING – FIELD PLOTS
CONSTANT CROWN HEIGHT, VARYING FILM THICKNESS

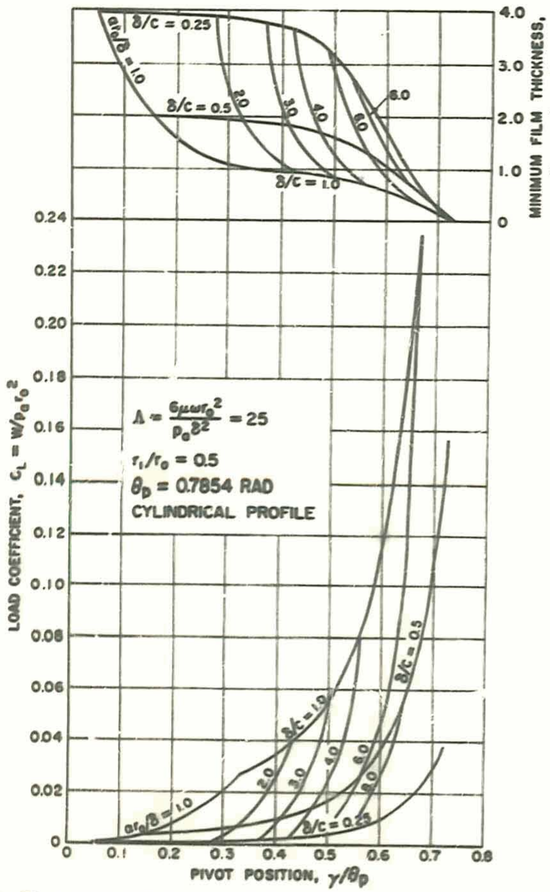

Fig. 14 Load Coefficient and Minimum Film Thickness vs. Pivot Position, Constant Crown Height, Varying Film Thickness, $\Lambda = 25$

TILTING PAD THRUST BEARING – FIELD PLOTS
CONSTANT CROWN HEIGHT, VARYING FILM THICKNESS

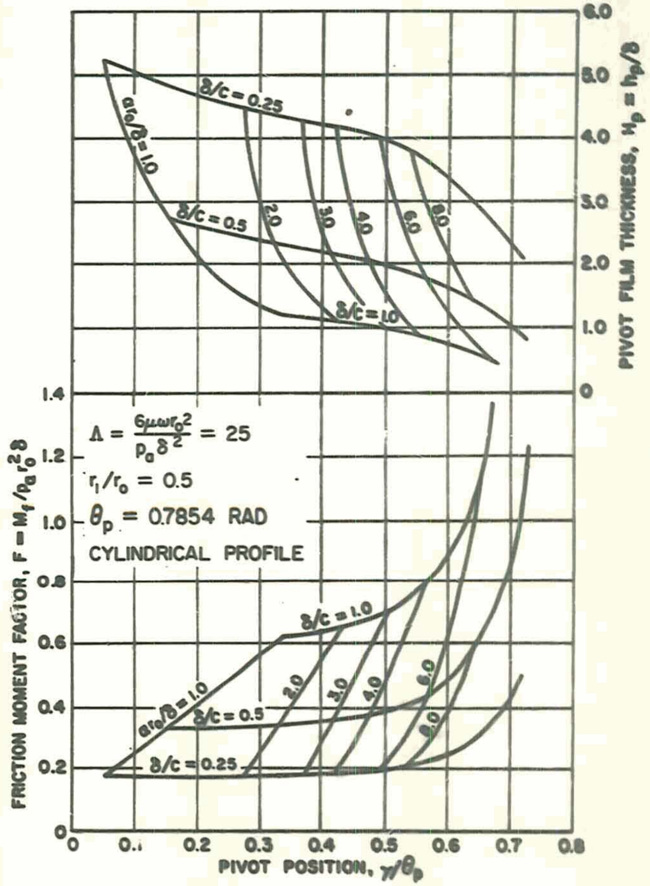

Fig. 15 Friction Moment Factor and Pivot Film Thickness vs. Pivot Position, Constant Crown Height, Varying Film Thickness, $\Lambda = 25$

TILTING PAD THRUST BEARING – FIELD PLOTS
CONSTANT CROWN HEIGHT, VARYING FILM THICKNESS

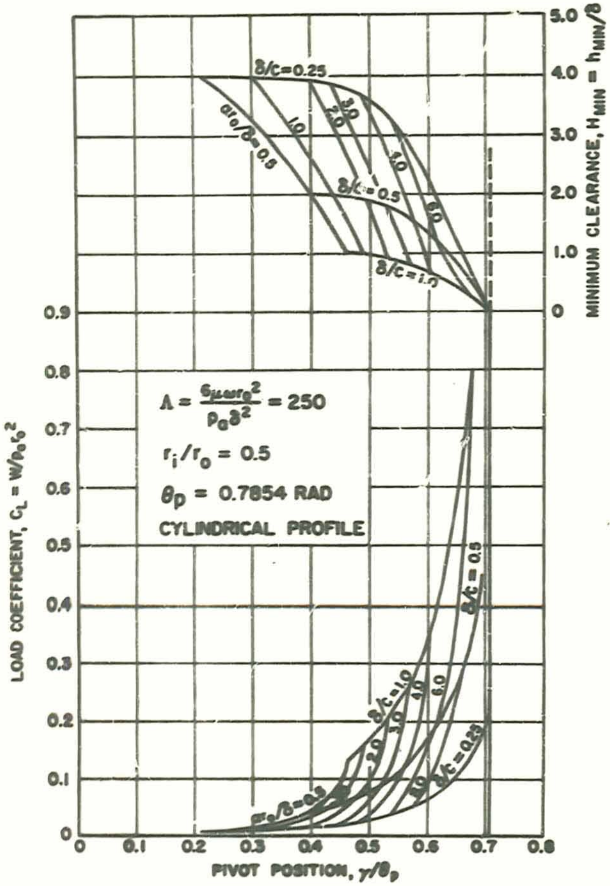

Fig. 16 Load Coefficient and Minimum Film Thickness vs. Pivot Position, Constant Crown Height, Varying Film Thickness, Λ = 250

TILTING PAD THRUST BEARING – FIELD PLOTS
CONSTANT CROWN HEIGHT, VARYING FILM THICKNESS

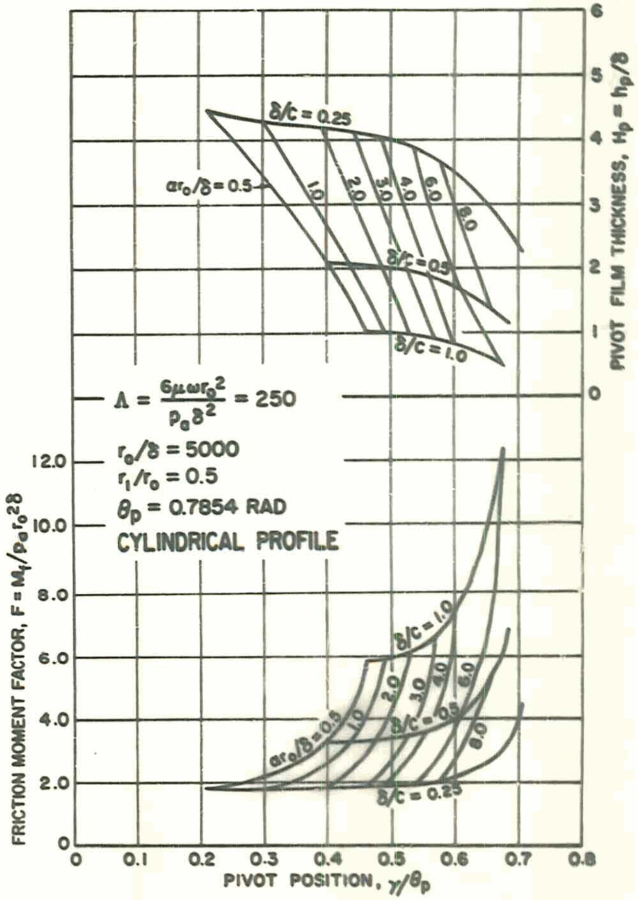

Fig. 17 Friction Moment Factor and Pivot Film Thickness vs. Pivot Position, Constant Crown Height, Varying Film Thickness, Λ = 250

TILTING PAD THRUST BEARING – FIELD PLOTS
CONSTANT CROWN HEIGHT, VARYING FILM THICKNESS

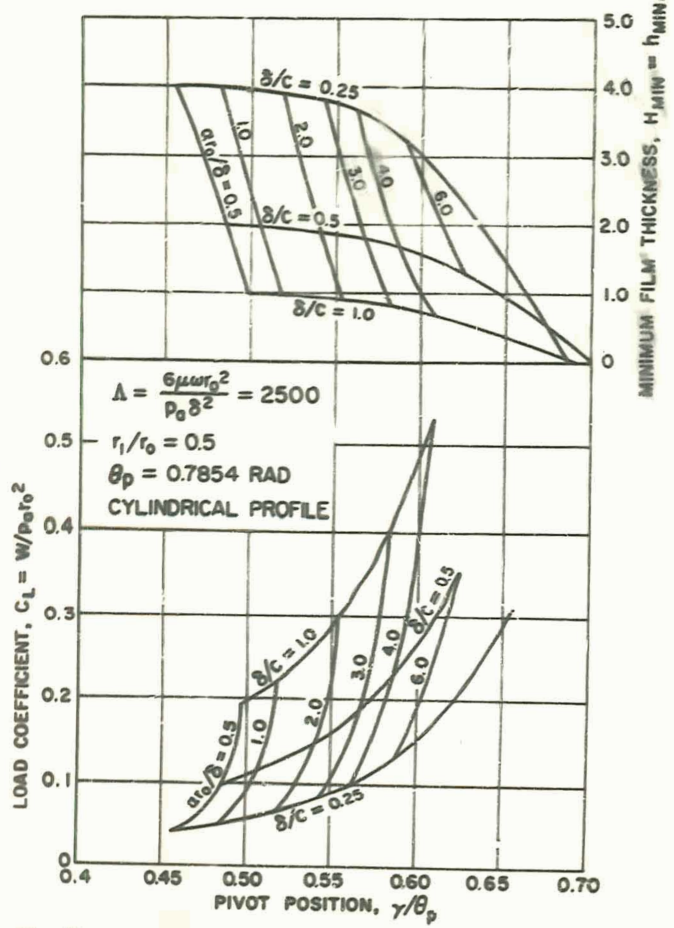

Fig. 18 Load Coefficient and Minimum Film Thickness vs. Pivot Position, Constant Crown Height, Varying Film Thickness, Λ = 2500

TILTING PAD THRUST BEARING – FIELD PLOTS
CONSTANT CROWN HEIGHT, VARYING FILM THICKNESS

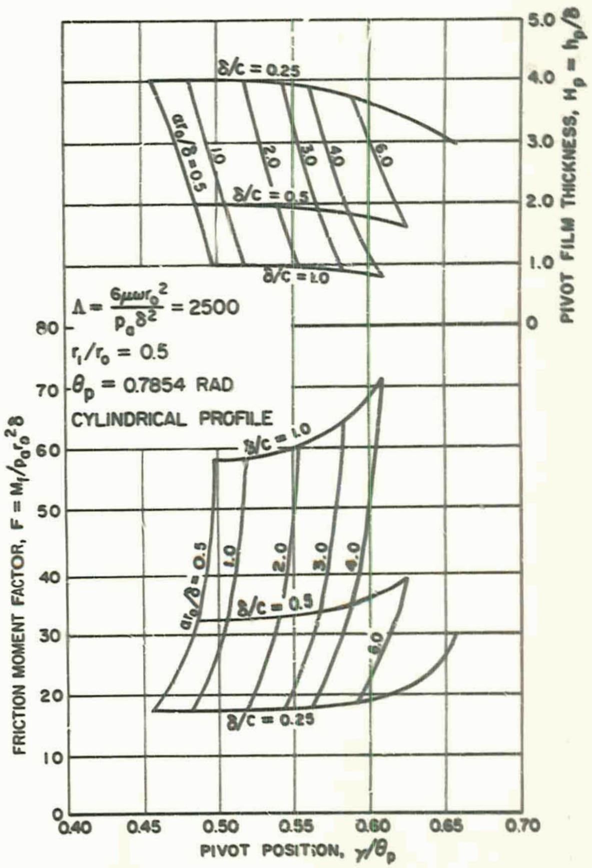

Fig. 19 Friction Moment Factor and Pivot Film Thickness vs. Pivot Position, Constant Crown Height, Varying Film Thickness, Λ = 2500

10. VARIATION OF PERFORMANCE WITH COMPRESSIBILITY PARAMETER, Λ

The variation of load coefficient with Λ is shown on Figure 20, at various values of minimum film thickness. The studies were made for a specific value of δ/c = 1.0. An almost linear relation persists up to a value of Λ = 20, then the load variation levels off, and begins to asymptotically approach a limiting value. The Friction Moment Factor (Figure 21) continues to rise linearly, however. The net result is that at the higher Λ values small gains in load capacity are obtained at the expense of a disproportionate increase in the Friction Moment Factor.

TILTING PAD THRUST BEARING – EFFECT OF VARYING Λ

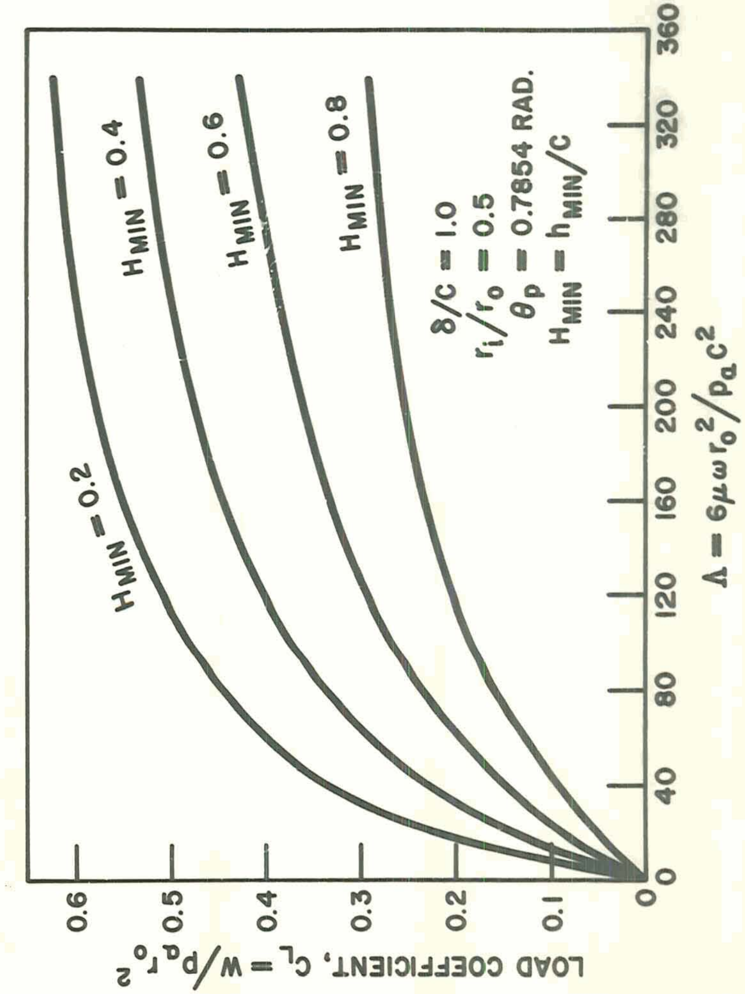

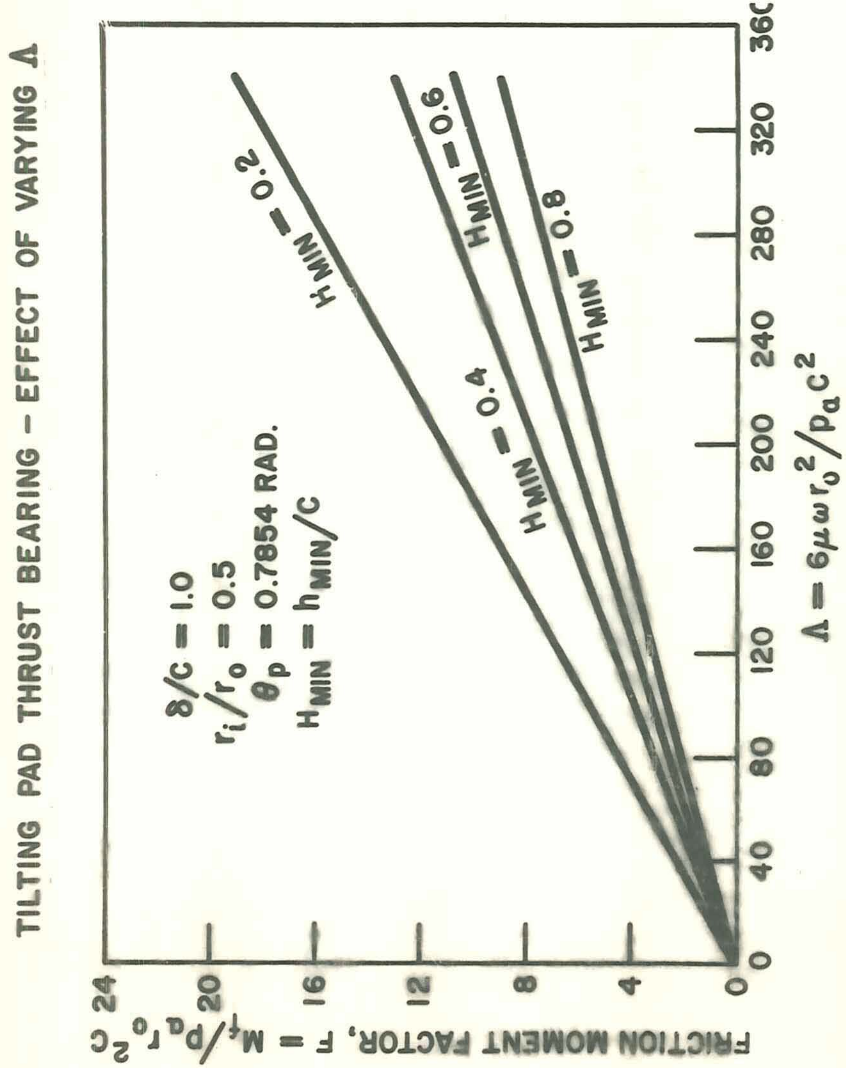

Fig. 21 Variation of Friction Moment Factor with Λ

11. DESIGN PROCEDURE

Although information has been limited to a specific pad configuration certain design procedures become evident. In most problems the load, geometry, viscosity and speed are specified.

1. Compute the Load Coefficient for maximum operating load.
2. Enter a curve such as Figure 20 and select a Λ between 120 and 250.
3. Establish H_{min} from Figure 20.
4. Compute c from known value of Λ.
5. Use a δ/c value equal to 1 and thus the crown height δ equals c for maximum loading.
6. From H_{min} and c, compute minimum film thickness h_{min} and insure it is reasonable for the application.
7. Compute Friction Moment Factor from a curve such as Figure 21.
8. Establish pivot position from field plots or other curves such as Figure 13 or Figure 14.
9. Using field plots determine off design performance by maintaining constant pivot position. With various values of δ/c or $\alpha r_o/\delta$ and load determine variation in minimum film thickness, friction moment and pivot film thickness.
10. Make adjustments as necessary to satisfy limitations.

The above procedure is intended as a guide in the use of the design information presented. There are many ramifications of the given information which would require appropriate changes to the procedures. Also, since some data is presented for specific values of Λ, δ/c, $\alpha r_o/c$ etc., cross plotting may be required or else designs limited to the parameters computed and plotted.

As an example of the above design procedure, consider the following sample problem.

<u>Given</u>

r_i = 2"

r_o = 4"

θ_p = 45^o

μ = 3.19×10^{-9} reyns $\left(\frac{\text{lb-sec}}{\text{in.}^2}\right)$ – air at 212°F

N = 20,000 rpm (ω = 2094 rad/sec)

p_a = 15 psia

W_T = 450 lbs (max)

Use 6 pads. W = 450/6 = 75 lbs/pad.

1. Load Coefficient $C_L = \frac{w}{p_a r_o^2} = 0.3125$

2. Select Λ = 250

3. From Figure 20 H_{min} = 0.732

4. $c = \sqrt{\frac{6\mu\omega r_o^2}{p_a \Lambda}} = 0.414 \times 10^{-3}$

5. $\delta/c = 1$, therefore $\delta = 0.414 \times 10^{-3}$

6. $h_{min} = H_{min} \times c = .303 \times 10^{-3}$ in.

7. From Figure 21 at Λ = 25[illegible] H_{min} = 0.732
   The Friction Moment Factor, F = 6.75

   $M_f = F \times p_a r_o^2 \delta$ = .6699 in.-lbs/pad

   M_f (6 pads) = 4.0194 in.-lbs.

   HP = Viscous horsepower = $\frac{M_f N}{63,000}$ = 1.276

8. Pivot Position
   From Figure 16 at C_L = 0.3125, δ/c = 1.0

$$\frac{\gamma}{\theta_p} = 0.585 \quad \text{for } \theta_p = 0.7854$$

$$\gamma = 0.4595 \text{ rad} = 26.33°$$

Also $\frac{\alpha r_o}{\delta} = 3.625$

$$\alpha = 3.625 \times \frac{\delta}{r_o} = 0.3747 \times 10^{-3} \text{ rad.}$$

From Table 2, $r_{pv}/r_o = 0.767$, r_{pv} = 3.068 in.

9. Pivot film thickness

   From Figure 17 at δ/c = 1 and $\frac{\gamma}{\theta_p}$ = 0.585

   $H_p = h_p/\delta = 0.857$

   $h_p = 0.3544 \times 10^{-3}$ in.

Design performance for other than maximum load conditions can be obtained by entering Figures 16 and 17 and following along a line of constant pivot position. Table 3 below summarizes some of the dimensionless parameters extracted from the curves and the computed dimensional performance.

TABLE 3

H_{min}	C_L	δ/c	$\alpha r_o/\delta$	F	H_p	W_T (lbs)	C (mils)	h_{min} (mils)	M_f (total) in-lbs	h_p (mils)	$\alpha \times 10^{-4}$ (rad)	HP
1.0	0.250	0.670	3.85	5.62	1.10	360	0.617	0.414	3.346	0.455	3.98	1.062
1.5	0.155	0.495	4.90	4.00	1.81	223	1.197	0.620	2.382	0.748	5.06	0.756
2.0	0.130	0.333	6.00	3.50	2.50	187	1.242	0.827	1.787	1.034	6.20	0.661
2.5	0.070	0.250	8.00	2.22	3.70	101	1.654	1.033	1.191	1.530	8.27	0.420

Figure 21a shows the variation of load capacity W_T, Friction Horsepower HP and pivot film thickness hp as a function of the minimum film thickness h_{min}.

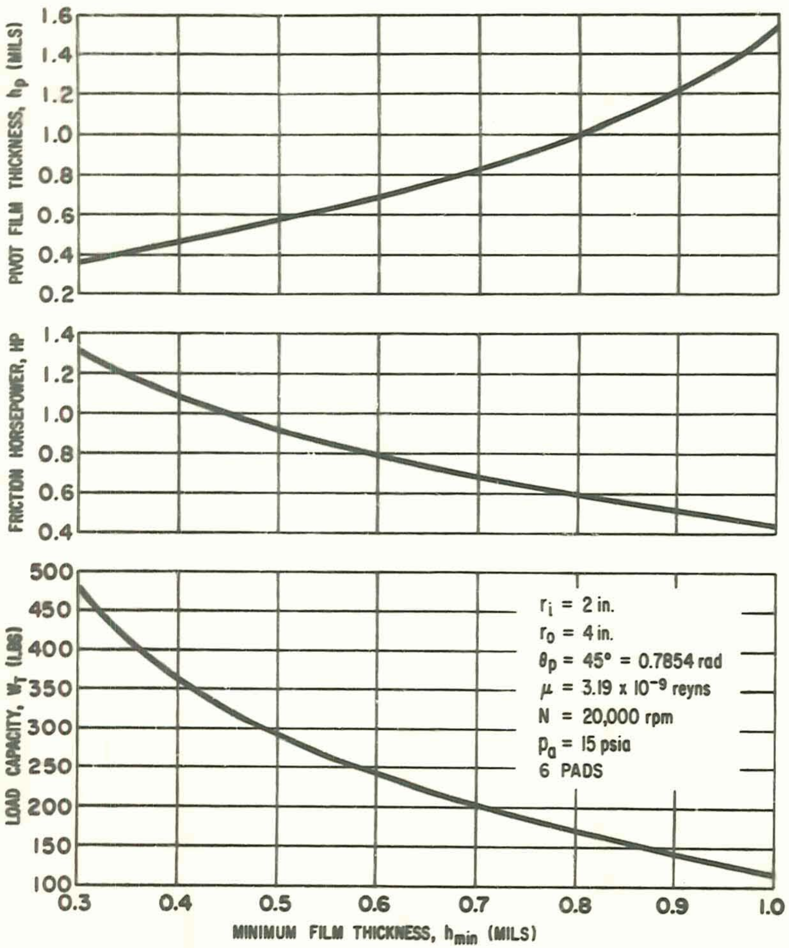

Fig. 21a Performance Curves, Sample Problem

12. LIMITATIONS OF INCOMPRESSIBLE THEORY

For small values of Λ, it is often permissable to use compressible theory to solve incompressible problems or vice versa. It is useful to know the degree of inaccuracy in this procedure, and where the bounds of applicability lie. When considering the incompressible case, the fluid may or may not cavitate in divergent film thickness regions, depending upon the ambient pressure.

Figure 22 shows comparative results between the compressible and incompressible cases for a parabolic profile at two different values of minimum film thickness. The incompressible theory, because of the linearity of the governing equations shows a linear variation with Λ. At low values of Λ the compressible load coefficient is higher, but at the higher values it falls off rapidly compared to the incompressible case. Further conclusions that can be drawn are as follows:

1. Cavitating incompressible theory is closer to compressible theory within the range of Λ's acceptable to both theories. This conclusion is somewhat anamalous since compressible theory might be expected to be more closely associated with the non-cavitating bearing because film rupture cannot occur and pressures can go below ambient. However, a cavitating pad with liquid lubricant has greater load capacity than the non-cavitating pad because negative pressures reduce load capacity. Thus, the cavitating pad more closely resembles the higher capacity compressible pad than the non-cavitating case.

2. The range of useful Λ's for interchangeability of theory varies as film thickness. The lower the film thickness, the lower the permissable value of Λ.

3. It appears that values of Λ less than 50 permit use of either theory.

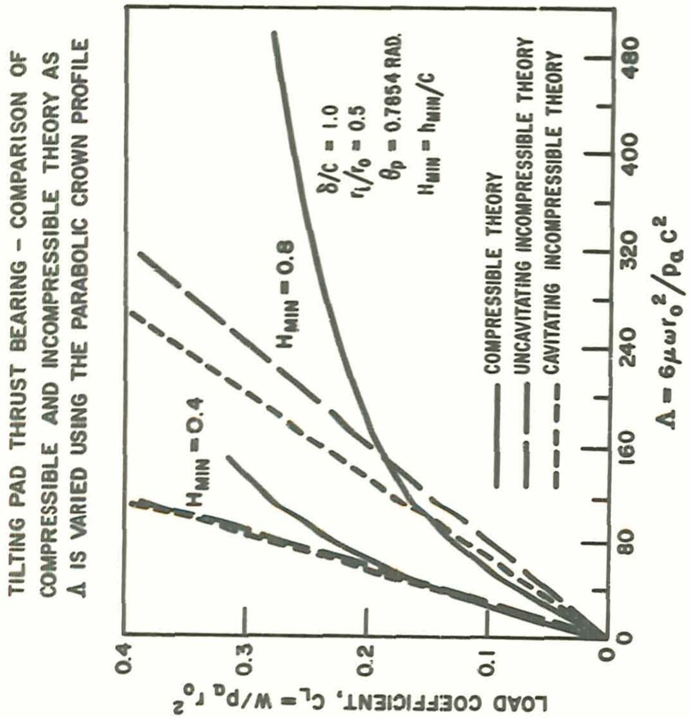

Fig. 22 Comparison of Load Coefficient for Incompressible and Compressible Theory vs. Λ

13. THE RECTANGULAR APPROXIMATION

Most of the published performance information on tilting-pad thrust bearings treat rectangular sliders. The transformation from a pie-shaped sector is made by assuming the rectangular length equal to the mean circumference of the sector, and the width equal to the difference between the inner and outer radii. The validity of the approximation was tested for two cases, one incompressible and the other compressible. For the incompressible case, separate analyses in the form of digital computer programs exist and precise comparisons were made. A flat pad profile was considered. Figure 23 shows the variation in load coefficient with minimum film thickness for the rectangular and pie-shaped sectors. Although Λ is shown as a parameter for the incompressible performance, the linear relationship permits elimination of this variable. The load coefficient divided by Λ is analogous to an inverse Sommerfeld Number. The Λ was retained in this instance to maintain the same format as for the compressible fluid pads. A fairly large error is introduced by the rectangular sector, which increases as the minimum film thickness is reduced. The error is not only due to the differences in hydrodynamic profile, but also due to the fact that for the same tilt the minimum film thickness of the rectangular sector is greater than for the pie-shaped sector. Alternatively, at the same minimum film the rectangular sector requires a greater tilt to support an equal load. With respect to load capacity, the rectangular approximation is over optimistic and thus may be misleading. Closer results can be obtained by computing the minimum film thickness of the actual sector, and then calculating the load on the basis of the rectangular information. The circles on Figure 23 represent load vs. minimum film thickness determined in this manner. The results are reasonably close to the actual pie-shaped sector performance, and are slightly pessimistic so that a safety factor is included.

Figure 24 are plots of Friction Moment Factor vs. Minimum Film Thickness for the incompressible case. Here the rectangular approximation gives conservative results at low values of film thickness, and over optimistic results at the higher film thickness magnitudes. Using the pie-shaped sector film in combination with the rectangular values of friction produces an almost parallel curve to the true sector except the predicted friction is too low Figures 25 and 26 show variations in load and friction as a function of angular tilt. This is another common way of plotting results. The pie-shaped and rectangular curves for load and friction are reasonably close and on this basis the rectangular approximation is good, but misleading because minimum film thicknesses can be considerably different.

Figures 27 through 30 are similar curves for a parabolic crowned pad operating with a compressible lubricant. By using large radii and maintaining the difference between the radii equal to the pad width a good approximation to the rectangular pad was obtained with the program that analyzes the pie-shaped sector. The section dealing with verification of the numerical analysis (Section 4) has already demonstrated the effectiveness of this approach.

The results are similar to the incompressible case. Perhaps a higher value of Λ, would have exhibited more clearly defined variations between trends of the incompressible and compressible lubricants.

The following general conclusions can be made concerning the rectangular approximation.

1. On the basis of actual minimum film thicknesses for the pie-shaped and rectangular pads, the rectangular approximation.

   (a) will give over-optimistic results for load capacity.

   (b) will give over-optimistic results for viscous friction at high minimum films, and conservative results at lower minimum films.

2. On the basis of pie-shaped minimum film thickness and rectangular performance, load capacity predictions will be conservative and viscous friction will be optimistic.

3. Comparisons using equal angular tilts produce reasonably good results, being conservative for load capacity and optimistic for viscous friction. These results can be misleading however because minimum films can be considerably different.

4. As r_i/r_o gets larger, the rectangular approximation should improve. There was no attempt to ascertain these effects, or to determine variations with Λ, and geometry.

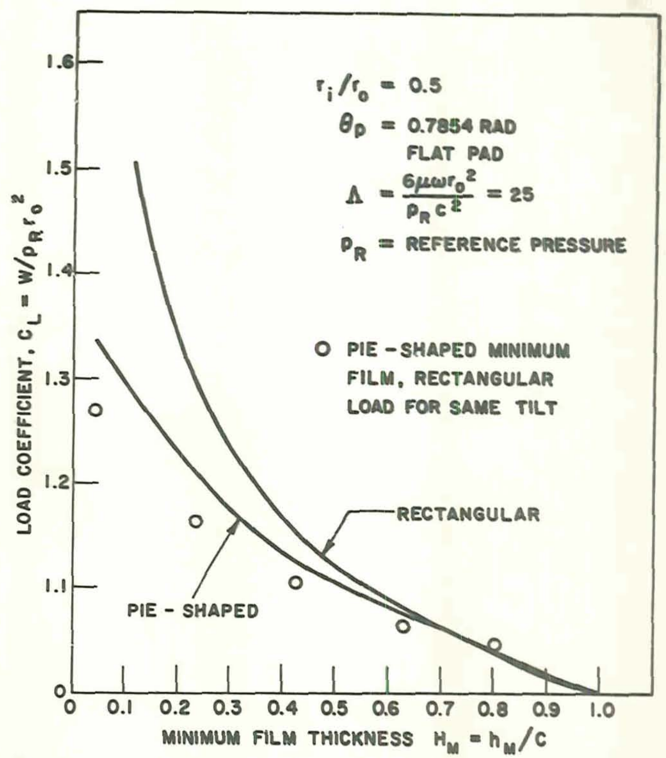

Fig. 23 Comparison Between Pie-Shaped Sector and Rectangular Approximation - Load Coefficient vs. Minimum Film Thickness - Incompressible Fluid

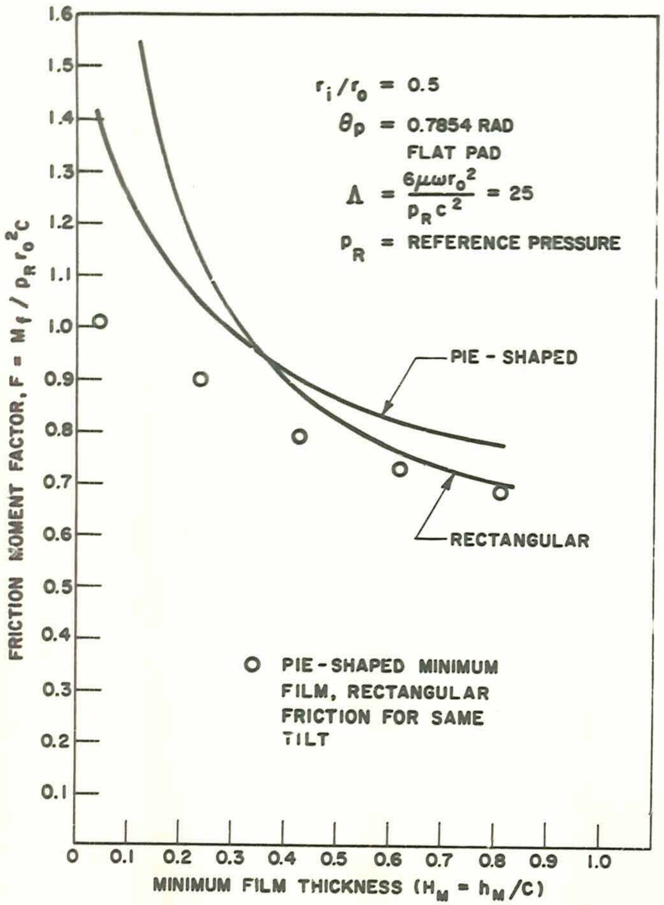

Fig. 24 Comparison Between Pie-Shaped Sector and Rectangular Approximation - Friction Moment Factor vs. Minimum Film Thickness - Incompressible Fluid

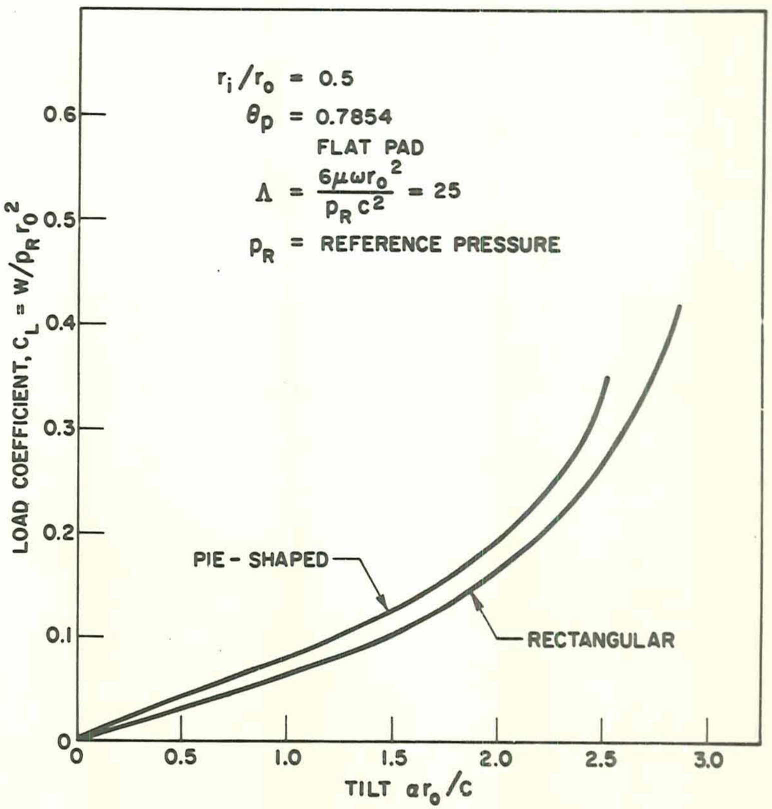

Fig. 25 Comparison Between Pie-Shaped Sector and Rectangular Approximation - Load Coefficient vs. Tilt-Incompressible Fluid

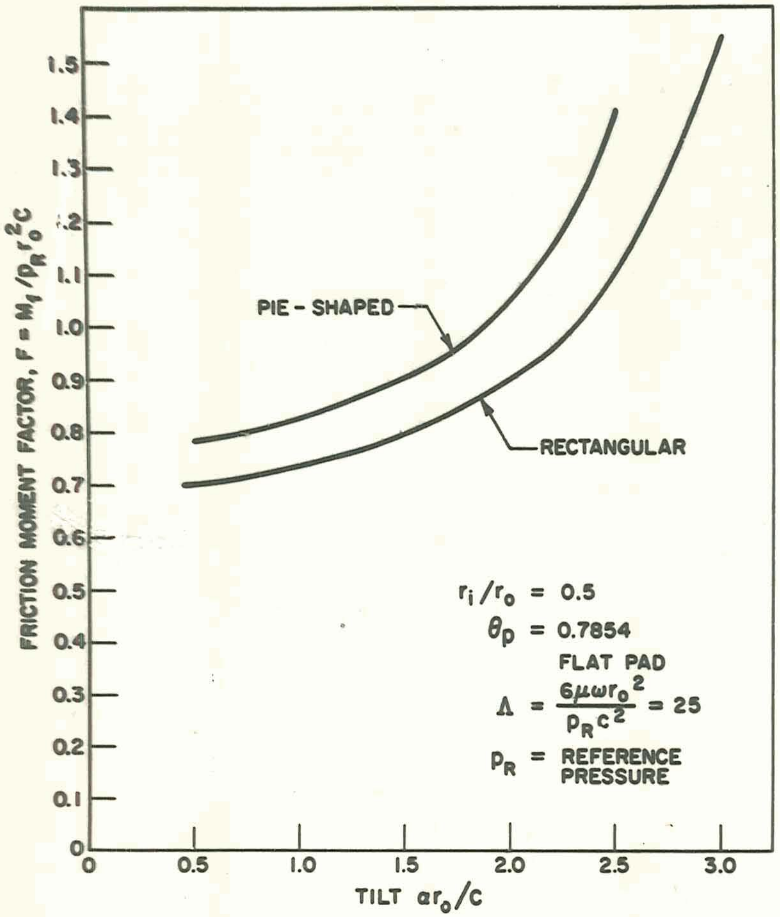

Fig. 26 Comparison Between Pie-Shaped Sector and Rectangular Approximation - Friction Moment Factor vs. Tilt-Incompressible Fluid

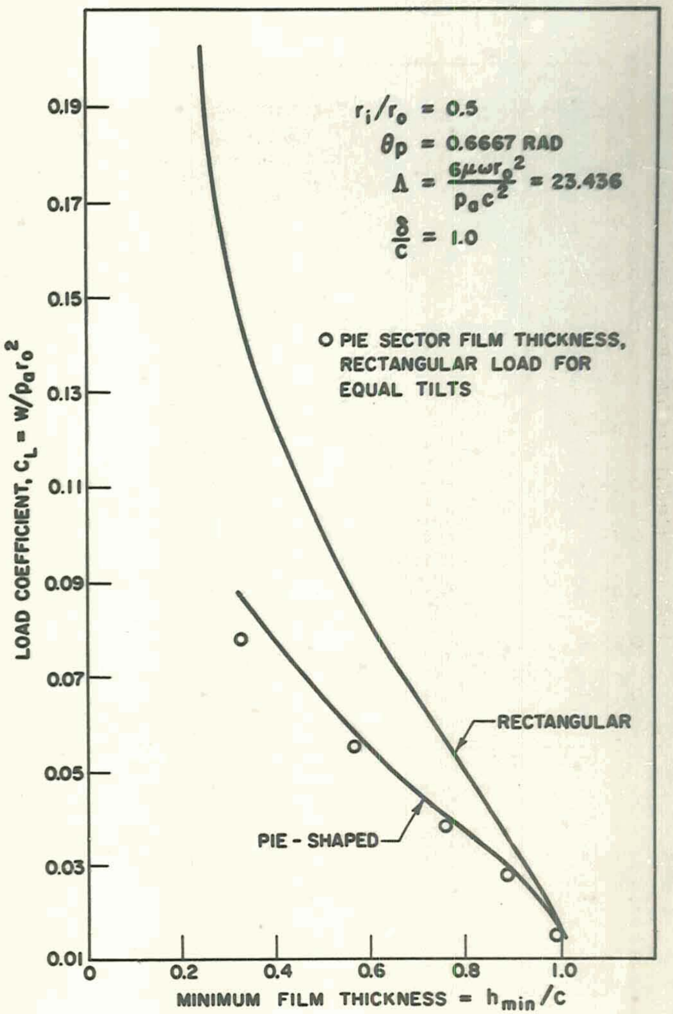

Fig. 27 Comparison Between Pie-Shaped Sector and Rectangular Approximation - Load Coefficient vs. Minimum Film Thickness - Compressible Fluid

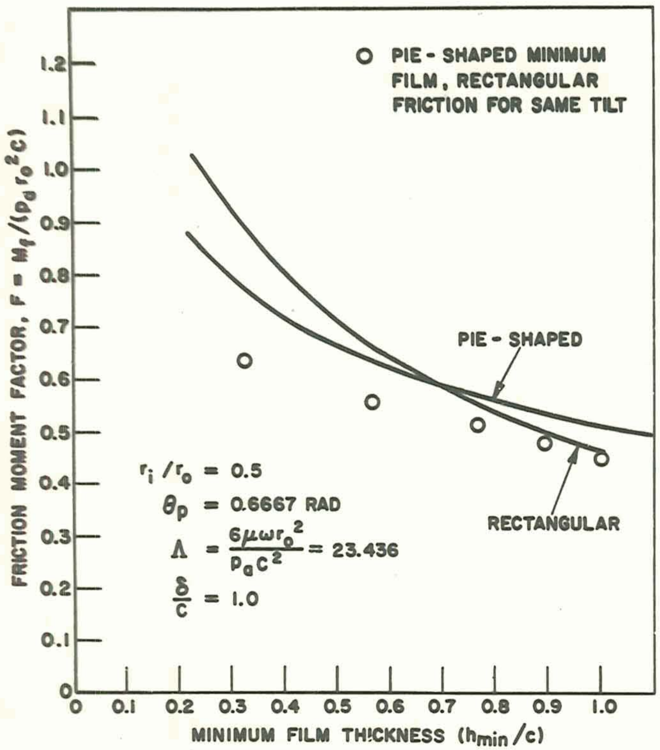

Fig. 28 Comparison Between Pie-Shaped Sector and Rectangular Approximation - Friction Moment Factor vs. Minimum Film Thickness - Compressible Fluid

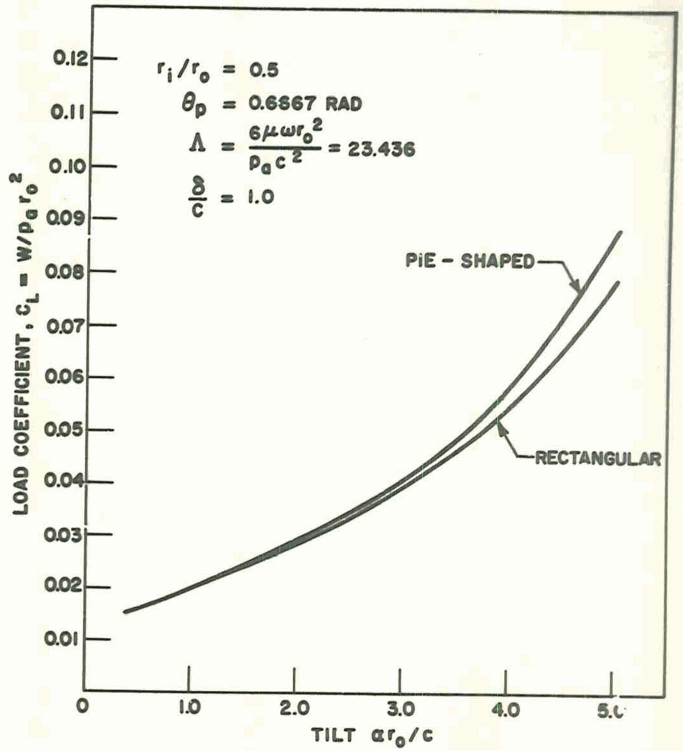

Fig. 29 Comparison Between Pie-Shaped Sector and Rectangular Approximation - Load Coefficient vs. Tilt-Compressible Fluid

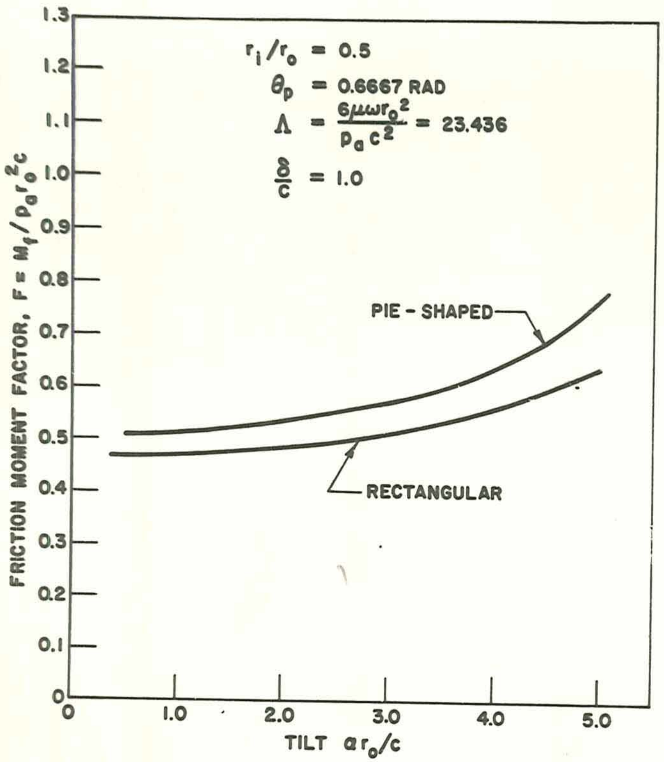

Fig. 30 Comparison Between Pie-Shaped Sector and Rectangular Approximation - Friction Moment Factor vs. Tilt-Compressible Fluid

14. SUMMARY

A computerized numerical analysis applied to the tilting pad thrust sector operating with compressible lubricants has been developed. Extensive performance information relating to a specific geometry has been presented along with optimization procedures. Limitations of various approximations have been clarified.

15. ACKNOWLEDGEMENTS

The authors express their gratitude to Professor D. D. Fuller for his guidance and helpful suggestions during the course of the investigation. The work represents a portion of Contract Nonr-2342 jointly sponsored by the Department of Defense, Atomic Energy Commission and The National Aeronautics and Space Administration. Mr. S. Doroff of the Fluid Dynamics Branch of the Office of Naval Research was contract administrator and his continuing encouragement and support of gas bearing development has significantly contributed to its rapidly expanding application.

W. Shapiro
W. Shapiro
Sr. Staff Engineer

R. Colsher
R. Colsher
Research Engineer II

Approved by:

Otto Decker
O. Decker, Manager
Friction & Lubrication Laboratory

Z. Zudans
Z. Zudans
Technical Director
Mechanical and Nuclear
Engineering Department

16. REFERENCES

1. *"Thermal Distortion of Spiral-Grooved Gas-Lubricated Thrust Bearing Due to Self Heating"*, C. H. T. Pan, B. Sternlicht, Trans. of ASME, Journal of Lubrication Technology, Volume 89, Series F, No. 2, April 1967, pp. 197-202.

2. *"Equilibrium Characteristics of Axial-Groove Gas-Lubricated Bearings"*, V. Castelli, J. Pirvics, Trans. of ASME, Journal of Lubrication Technology, Volume 89, Series F, No. 2, April 1967, pp. 177-196.

3. *"Gas Film Lubrication"*, W. A. Gross, John Wiley and Sons, Inc., Copyright 1962.

DOCUMENT CONTROL DATA - R&D

(Security classification of title, body of abstract and indexing annotation must be entered when the overall report is classified)

1. ORIGINATING ACTIVITY (Corporate author) The Franklin Institute Research Laboratories 20th and the Benjamin Franklin Parkway Philadelphia, Pennsylvania 19103	2a. REPORT SECURITY CLASSIFICATION UNCLASSIFIED 2b. GROUP None

3. REPORT TITLE

Analysis and Performance of the Gas-Lubricated Tilting Pad Thrust Bearing

4. DESCRIPTIVE NOTES (Type of report and inclusive dates)

Interim Report October 1968

5. AUTHOR(S) (Last name, first name, initial)

Shapiro, W.
Colsher, R.

6. REPORT DATE	7a. TOTAL NO. OF PAGES	7b. NO. OF REFS
October 1968	60	3

8a. CONTRACT OR GRANT NO. Nonr-2342(00) b. PROJECT NO. c. Task NR -62-316 d.	9a. ORIGINATOR'S REPORT NUMBER(S) I-A2049-30 9b. OTHER REPORT NO(S) (Any other numbers that may be assigned this report)

10. AVAILABILITY/LIMITATION NOTICES

Reproduction in Whole or in Part is Permitted for any Purpose of the U.S. Government

11. SUPPLEMENTARY NOTES	12. SPONSORING MILITARY ACTIVITY
--	--

13. ABSTRACT

The inherent self aligning capability and superior resistance to thermal distortion, of the gas-lubricated tilting-pad thrust bearing could often offset load capacity limitations and make it an attractive compromise for many applications. A numerical treatment for analyzing the tilting-pad thrust bearing is presented along with extensive performance information for a particular pad geometry. An optimum hydrodynamic crown profile and related dimensions are determined. The range of validity of incompressible theory and the rectangular approximation are also developed. ()

DD FORM 1 JAN 64 1473

END

DATE

FILMED

2-1-69